Role of fast sputtered particles during sputter deposition: Growth of epitaxial $Ge_{0.99}C_{0.01}$/Ge(001)

J. D'Arcy-Gall, D. Gall, P. Desjardins, I. Petrov, and J. E. Greene
Materials Science Department and the Frederick Seitz Materials Research Laboratory, University of Illinois, 104 South Goodwin Avenue, Urbana, Illinois 61801

(Received 12 May 2000; revised manuscript received 5 July 2000)

We show that fast sputtered particles in the sputter-deposition process, largely ignored in previous studies, can play a major role in determining defect densities in as-deposited layers. Epitaxial $Ge_{1-y}C_y$/Ge(001), in which there is a direct correlation between C lattice configurations and the local concentration of Ge self-interstitials, is used as a model materials system. We show that increasing the fraction of fast Ge neutrals in the high-energy tail of the ejected particle distribution increases the concentration of Ge–C split interstitials and thus the film compressive strain. The Ge–C split interstitials form as a result of trapping, by incorporated substitutional C atoms, of Ge self-interstitials produced by incident hyperthermal Ge atoms. Experimental results are supported by Monte Carlo simulations and *ab initio* calculations.

I. INTRODUCTION

Energetic ion irradiation is commonly used for *in situ* processing during film deposition. It has been shown, for example, to provide higher-packing densities during film growth at low temperatures,[1–3] increased nucleation rates,[4] enhanced preferred orientation,[1,5] controlled changes in alloy film compositions,[6] and enhanced dopant incorporation probabilities.[7,8] Most studies have focused on the effects of relatively high energy ($\geqslant$100 eV) inert and/or reactive ion irradiation, which often lead to unintentional side effects including substantial residual defect concentrations[9] and high-compressive stresses in as-deposited layers.[10] The experiments have typically been carried out using bias sputter deposition, in which a negative potential is applied to the substrate in order to extract positive ions from the plasma, or ion-beam assisted deposition employing a separate ion beam coincident with the deposited film flux. In the latter case, the deposition flux originates from either an evaporative or a sputter source.

In all sputter-deposition processes, there is an additional source of hyperthermal species—the sputtered species themselves—to which relatively little attention has been paid. At low operating pressures, typical of magnetron or ion-beam sputtering, depositing species are incident with average translational energies of the order of, or larger than, surface bond energies but generally smaller than bulk displacement energies E_d (typically 15 to 20 eV for metals and semiconductors). However, there is a high-energy tail in the sputtered atom distribution with energies extending up to hundreds of eV. These high-energy particles can be expected to play a role in determining film properties.

Nevertheless, few studies have focused on the effects of momentum transfer from fast sputtered atoms to the film growth surface. Molecular-dynamic simulations by Kitabatake, Fons, and Greene[11] show that growth of Si(001) from 10 eV Si atoms results in the formation of self-interstitials, which are distributed over 6 layers, while growth from 50 eV Si beams[12] yields both self-interstitials and vacancies over 14 and 7 layers, respectively. The simulations also indicate that the point defects, at typical epitaxial Si growth temperatures, are annealed out during deposition. This is consistent with experimental observations that homoepitaxial Si(001):Sb (Ref. 13) and Ge(001):Al (Ref. 14) layers grown at 400 °C from hyperthermal beams with average energies of 18 and 12 eV, respectively, exhibit carrier mobilities equal to or better than reported values for bulk Si and Ge.

The present experiments were undertaken to investigate defect creation induced by irradiation from hyperthermal sputtered species during film growth. Ion-beam sputter deposition (IBSD) is a well-suited method for this since the discharge is confined in the ion source, thus eliminating interactions between the primary ions and the growing film. However, the layers still receive high fluxes of energetic particles, due to primary ions that are neutralized just prior to being backscattered from the target, often with sufficient energy to cause defect formation and residual stress in as-deposited layers.[15] We have essentially eliminated this irradiation source as well by careful design of system geometry, utilizing the fact that ions incident at the target at oblique angles are primarily forward scattered, and the choice of relative ion/target atom masses.[14]

In this paper, we provide experimental evidence that fast sputtered neutrals in the sputter-deposition process can play a major role in determining point defect densities in as-deposited layers. We change the primary ion energy during ultrahigh vacuum IBSD to vary the high-energy tail of the sputtered atom distribution $dN(E)/dE$ while maintaining the average energy $\langle E \rangle$ of incident depositing particles essentially constant. Epitaxial $Ge_{1-y}C_y$ layers grown on Ge(001) are used as a model materials system since C atom lattice sites depend sensitively on the concentration of Ge self-interstitials.[16,17] C-containing Group-IV semiconductor alloys are themselves of interest due to the potential they offer for both band gap and strain engineering in microelectronics. We show that the strain state of coherent epitaxial $Ge_{0.99}C_{0.01}$ alloy layers grown on Ge(001) at $T_s = 300$ °C using Kr^+ ion-beam sputter deposition from Ge and C targets, continuously varies from in-plane tension to in-plane compression as the primary ion energy E_{Kr} is increased from 300 to 900 eV. The change in strain state is due to an increasing fraction of C becoming incorporated in Ge–C split interstitial sites as a result of the trapping, by substitutional C, of Ge

self-interstitials formed due to fast Ge irradiation. The results are supported by TRIM Monte Carlo simulations indicating that the number of lattice displacements per incident hyperthermal Ge atom, dpa, increases rapidly with E_{Kr} due to the increasing fraction of Ge atoms in the high-energy tail of $dN(E_{\mathrm{Ge}})/dE_{\mathrm{Ge}}$.

II. EXPERIMENTAL PROCEDURE

All film growth experiments were conducted in an ultrahigh-vacuum (UHV) load-locked multichamber stainless-steel system with a base pressure of 1×10^{-10} Torr.[18] Kr^+ ions with kinetic energies $E_{\mathrm{Kr}}=300-900$ eV were used to sputter undoped float-zone Ge and high-purity C targets in order to generate hyperthermal Ge and C fluxes. Sputtering is carried out using two modified UHV Kaufman-type double-grid multiaperture broad ion-beam sources with provisions for *in situ* spatial adjustment. A detailed discussion of the design, construction, and operation of the ion sources is presented elsewhere.[14]

The Ge and C targets are suspended on an insulating cantilever and can be adjusted with respect to the substrate to exploit the angular distribution of fast backscattered Kr atoms and to optimize film-thickness uniformity. Each ion beam is focused by a postextraction unipotential electrostatic lens that also acts as a mirror to prevent electron backstreaming from the neutralization device. Space-charge spreading of each ion beam is suppressed immediately upon emerging from the final lens aperture by electron injection from a circular thermionic W filament. The filament is positioned external to the beam in order to eliminate W contamination.

$Ge_{1-y}C_y$ film compositions were controlled through the choice of beam currents from each ion gun. The use of the higher-mass Kr instead of Ar, together with single-crystal Ge apertures and the forward-scattering geometry described in Ref. 14, minimizes the flux of energetic backscattered Kr incident at the growing film. The Kr pressure in the chamber was 1.2×10^{-4} Torr during deposition.

The substrates were polished 1.5×1.5 cm^2 *n*-type Ge(001) wafers with room-temperature resistivities of 1–20 Ω cm ($n=1\times10^{15}$—6×10^{13} cm^{-3}). Substrate cleaning consisted of solvent degreasing followed by an ultraviolet ozone treatment, UHV degassing, and oxide desorption.[19] 1000-Å-thick Ge(001) buffer layers were then deposited at $T_s=400\,^{\circ}$C using $E_{\mathrm{Kr}}=900$ eV and a growth rate $R_{\mathrm{Ge}}=1.4$ Å s^{-1}. The resulting Ge(001) layers exhibit sharp 2×1 reflection high-energy electron diffraction (RHEED) patterns. $Ge_{0.99}C_{0.01}$ alloys were grown at $T_s=300\,^{\circ}$C using $E_{\mathrm{Kr}}=300-900$ eV for sputtering both the C and the Ge targets. R_{GeC} ranged from 0.3 to 1.4 Å s^{-1} and the deposition time was adjusted such that all samples are $\simeq$2000 Å thick. RHEED patterns remained 2×1 for all alloy layers.

$Ge_{1-y}C_y$ film compositions were determined using a Cameca IMS-5F secondary-ion mass spectrometer (SIMS) operated with a 10 kV Cs^+ primary ion beam. Quantification was obtained by comparison to C-implanted Ge(001) reference wafers. C concentrations in the deposited $Ge_{1-y}C_y$ layers were found by SIMS analyses to be constant to within experimental error, $\pm2\%$, as a function of depth, independent of E_{Kr}. No Kr was detected in any of the films.

The microstructure, strain-state, and crystalline quality of the $Ge_{1-y}C_y$ layers were determined by cross-sectional transmission electron microscopy (XTEM), high resolution x-ray diffraction (HR-XRD), and high-resolution reciprocal lattice mapping (HR-RLM). A Philips CM12 microscope operated at 120 kV was used for the XTEM examinations and specimens were prepared by mechanical thinning followed by ion milling as described in Ref. 20. Film lattice constants $a_\perp$ along the growth direction were obtained from HR-XRD ω-2θ measurements in a Philips MRD diffractometer using Cu $K_{\alpha I}$ radiation ($\lambda=1.540\,597$ Å) from a four-crystal Ge(220) monochromator. In-plane lattice constants $a_\parallel$ and residual strains were determined from HR-RLM's around asymmetric reflections. For the latter measurements, an additional two-crystal Ge(220) analyzer was placed in front of the detector and a series of ω-2θ scans was acquired at different ω offsets.

Prior to the growth of $Ge_{1-y}C_y$ alloys, pure Ge(001) layers were grown using the deposition conditions described above. XTEM and HR-XRD results show that the layers, even those deposited with the highest E_{Kr} values, were highly perfect single crystals as expected based upon previous results[13,14] and exhibited no measurable strain (detection limit $\simeq5\times10^{-4}$).

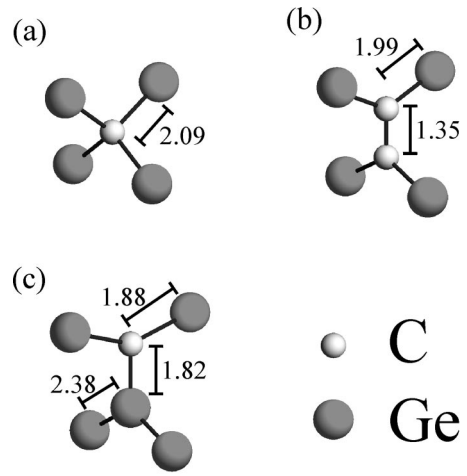

FIG. 1. Relaxed C configurations in pseudomorphic $Ge_{1-y}C_y$ with in-plane lattice constants $a_x=a_y=a_{\mathrm{Ge}}$; (a) a substitutional C, (b) a C pair, and (c) a Ge–C split interstitial. The bond lengths are in Å.

III. *AB INITIO* CALCULATIONS AND MONTE CARLO SIMULATIONS

We employed *ab initio* methods based on density-functional theory,[21] using the generalized gradient approximation[22] with 64-atom supercells, to determine formation energies U per C atom and out-of-plane strain coefficients α for C configurations in fully strained $Ge_{1-y}C_y$ alloys on Ge(001). We calculated the formation energy of $\simeq$20 configurations. Figure 1 shows the most stable configurations involving one and two C atoms. Substitutional C with $U_{\mathrm{sub}}=2.40$ eV and $\alpha_{\mathrm{sub}}=-0.71$ is shown in Fig. 1(a) while Fig. 1(b) is a [001]-oriented C pair occupying a single site in the Ge lattice with a formation energy per C atom of $U_{\mathrm{pair}}=2.23$ eV and a strain coefficient $\alpha_{\mathrm{pair}}=0.18$. The [001]-

oriented Ge-C split interstitial [Fig. 1(c)], formed by the capture of a Ge self-interstitial by a substitutional C, is the most stable interstitial C configuration in Ge and has a formation energy and strain coefficient of $U_{\text{split}}=4.18\,\text{eV}$ and $\alpha_{\text{split}}=0.95$, respectively. Thus, at equilibrium, the C pair is the most favorable configuration for C in the Ge lattice. However, substitutional C atoms are only slightly less favorable, with a formation energy that is 0.17 eV higher, while the formation energy of the Ge-C split interstitial is 1.95 eV greater than that of the C pair.

There is a tendency for the C–C and Ge–C dimers to align preferentially along [001] for fully coherent alloys in which the in-plane lattice constant is commensurate with that of the Ge substrate. Our calculations show, for example, that [001]-oriented Ge–C split interstitials are 0.1 eV more stable than those oriented along [100] or [010].

The out-of-plane lattice constant $a_\perp$ for completely coherent $Ge_{1-y}C_y$ films on Ge(001) can be expressed as a linear combination of the strains associated with C in each lattice configuration,

$$a_\perp = a_{\text{Ge}}(1+\alpha_{\text{sub}}y_{\text{sub}}+\alpha_{\text{pair}}y_{\text{pair}}+\alpha_{\text{split}}y_{\text{split}}). \qquad (1)$$

a_{Ge} in Eq. (1) is the relaxed bulk Ge lattice constant (5.6576 Å) while y_{sub}, y_{pair}, and y_{split} are the atomic fractions of C incorporated in substitutional pair and split-interstitial sites, respectively. For the limiting cases in which all C atoms in fully strained $Ge_{0.99}C_{0.01}$ alloys are incorporated in just one type of site, we calculate $a_\perp$ to be 5.617 Å (substitutional C), 5.668 Å (C pairs), and 5.711 Å (Ge–C split interstitials).

We performed TRIM[23] Monte Carlo simulations to estimate the total dpa created by fast Ge atoms incident at growing $Ge_{0.99}C_{0.01}(001)$ films due to Kr ion-beam sputtering of a Ge target with $E_{\text{Kr}}=300-900\,\text{eV}$, while accounting for our system geometry. We first calculate the energy distributions of sputtered Ge and C atoms with ejection angles that intercept the substrate and then use these results, together with a lattice displacement energy of $E_d=15\,\text{eV}$, appropriate for pure Ge,[24] as input parameters to determine total dpa. As discussed below, our simulations indicate that dpa values obtained by varying E_{Kr} from 300 to 900 eV are more than sufficient to give rise to measurable changes in film strain, even though TRIM simulations tend to underestimate dpa values for low-energy irradiation.[25]

Figure 2(a) shows calculated energy distributions $dN(E_{\text{Ge}})/dE_{\text{Ge}}$ of ejected Ge atoms due to target sputtering by 10^4 Kr ions with energies E_{Kr} of either 300 or 900 eV. Ge atoms, which are incident at 20° to the substrate surface normal, have average translational energies $\langle E_{\text{Ge}}\rangle$ of 13 eV ($E_{\text{Kr}}=300\,\text{eV}$) and 16 eV($E_{\text{Kr}}=900\,\text{eV}$). The two energy distributions in Fig. 2(a) are similar with the primary difference being in the high-energy tails. Table I lists the fraction of incident Ge atoms f_{Ge}, as a function of E_{Kr}, with E_{Ge} larger than 20, 50, 100, and 200 eV. All f_{Ge} values increase with increasing E_{Kr}. For example, $f_{\text{Ge}}(E_{\text{Ge}}\geqslant 50\,\text{eV})$ increases from 1.9% with $E_{\text{Kr}}=300\,\text{eV}$ to 4.5% with $E_{\text{Kr}}=900\,\text{eV}$. $f_{\text{Ge}}(E_{\text{Ge}}\geqslant 200\,\text{eV})$ increases by more than an order of magnitude over the same E_{Kr} range.

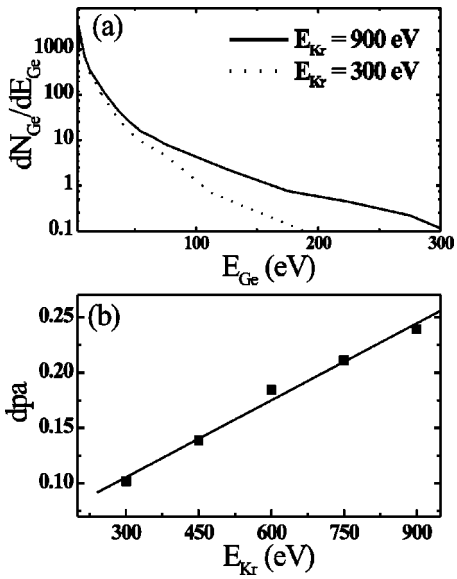

FIG. 2. (a) Normalized energy distributions $dN(E_{\text{Ge}})/dE_{\text{Ge}}$, plotted as the number of Ge atoms N_{Ge} per eV, as a function of the kinetic energy E_{Ge} of sputter-ejected Ge atoms incident at the growing $Ge_{0.99}C_{0.01}(001)$ film. The distributions were obtained from TRIM simulations, accounting for our experimental geometry, for 300 eV (dashed line) and 900 eV (solid line) Kr^+ ion irradiation of a Ge target. (b) Calculated lattice displacements per incident atom (dpa) in $Ge_{0.99}C_{0.01}$ layers due to incident energetic sputtered Ge atoms with the energy distributions calculated in (a) as a function of the Kr^+ ion energy E_{Kr} at the target.

For reference, Table II shows calculated dpa produced in Ge by bombardment with monoenergetic Ge atoms, at normal incidence, as a function of E_{Ge}. The dpa increases rapidly, from 0.39 at $E_{\text{Ge}}=25\,\text{eV}$ to 7.42 at 200 eV.

Incident particle energy distributions, including those shown in Fig. 2(a), were used as input parameters to calculate *total* dpa during $Ge_{0.99}C_{0.01}$ film growth. The contribution of incident hyperthermal C atoms to defect creation is negligible due to the combination of their much smaller mass and low flux. For example, the calculated dpa due to incident hyperthermal C atoms produced with $E_{\text{Kr}}=900\,\text{eV}$ is smaller

TABLE I. Calculated fraction of incident Ge atoms f_{Ge} having kinetic energies E_{Ge} over 20, 50, 100, and 200 eV, for different values of E_{kr}.

E_{kr} (eV)	$f_{\text{Ge}}(E_{\text{Ge}}\geqslant 20\,\text{eV})$	$f_{\text{Ge}}(E_{\text{Ge}}\geqslant 50\,\text{eV})$	$f_{\text{Ge}}(E_{\text{Ge}}\geqslant 100\,\text{eV})$	$f_{\text{Ge}}(E_{\text{Ge}}\geqslant 200\,\text{eV})$
300	0.107	0.0193	0.0020	0.0002
450	0.136	0.0264	0.0048	0.0008
600	0.151	0.0339	0.0091	0.0013
750	0.164	0.0394	0.0106	0.0019
900	0.173	0.0446	0.0135	0.0030

TABLE II. Calculated dpa vs incident Ge atom energy, E_{Ge}.

E_{Ge} (eV)	Dpa
15	0
25	0.39
50	1.41
100	3.48
200	7.42

than that due to fast Ge with $E_{Kr}=300$ eV. We therefore use only the Ge incident particle energy distribution in the calculation of the total dpa during film growth. The obtained dpa, plotted in Fig. 2(b), increases linearly by more than a factor of 2 as E_{Kr} is varied from 300 to 900 eV. The simulations also indicate that the amount of resputtering in the films is negligible, as less than 0.8% of the incident Ge atoms cause resputtering. Furthermore, our SIMS results show no measurable change in the C/Ge ratio as a function of E_{Kr}. The results of our TRIM simulations are used, as described below, to correlate changes in film strain as a function of E_{Kr} with point defect formation during IBSD.

IV. RESULTS AND DISCUSSION

All $Ge_{0.99}C_{0.01}(001)$ layers, irrespective of E_{Kr}, were found to be high-quality single crystals with no detectable extended defects. Figure 3 is a typical bright-field XTEM image, obtained using the diffraction vector $\bar{g}=220$ near the 110 zone axis, from a highly perfect fully coherent (as determined by HR-RLM, see below) $Ge_{0.99}C_{0.01}$ layer grown using $E_{Kr}=450$ eV (dpa$=0.14$). The film is flat to within the resolution of TEM. Strain contrast due to lattice constant mismatch is clearly observed at the film/buffer-layer interface. The [110] zone axis selected-area electron-diffraction pattern in the inset consists of single-crystal reflections with symmetric intensities.

All alloy layers are completely coherent with their substrates as determined from XTEM and HR-RLM analyses. Typical maps around the asymmetric 224 reflection from $Ge_{0.99}C_{0.01}$ layers grown with $E_{Kr}=300$ eV and 750 eV (dpa$=0.10$ and 0.21) are presented in Fig. 4. Diffracted intensities are plotted as isointensity contours as a function of the reciprocal lattice vectors $k_{\|}$ parallel and $k_{\perp}$ perpendicular to the surface. The substrate and the film peaks are essentially perfectly aligned along the $k_{\|}$ direction indicating negligible ($\leq 1\times10^{-5}$) in-plane strain relaxation. The diffraction contours are nearly symmetric except for the elongation along the growth direction due to finite-thickness effects. The lateral broadening of the layer peaks is comparable to that of the substrates indicative, in agreement with XTEM results, of the high structural quality of the $Ge_{0.99}C_{0.01}$ layers.

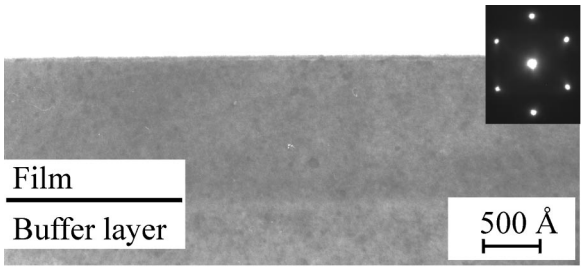

FIG. 3. A [110] bright-field XTEM image, obtained with diffraction vector $\bar{g}=220$, from a fully strained $Ge_{0.99}C_{0.01}$ alloy layer grown on Ge(001) at $T_s=300\,^{\circ}$C with $E_{Kr}=450$ eV. A 110 selected-area electron diffraction pattern is shown in the inset.

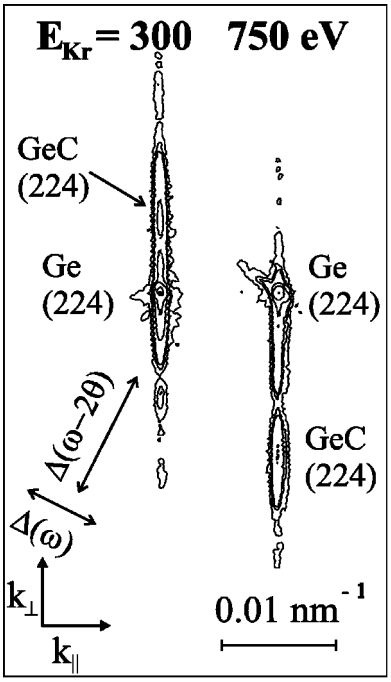

FIG. 4. High-resolution reciprocal lattice maps, obtained around the asymmetric 224 Bragg peaks, from $Ge_{0.99}C_{0.01}$ alloys grown on Ge(001) using $E_{Kr}=300$ and 750 eV.

Figure 5 is a plot of $a_{\perp}$ vs dpa for $Ge_{0.99}C_{0.01}$ layers. Alloys deposited with $E_{Kr}\leq 450$ eV (dpa≤ 0.14) are in tension with $a_{\perp}\simeq 5.65$ Å. Increasing E_{Kr} to 600 eV (dpa

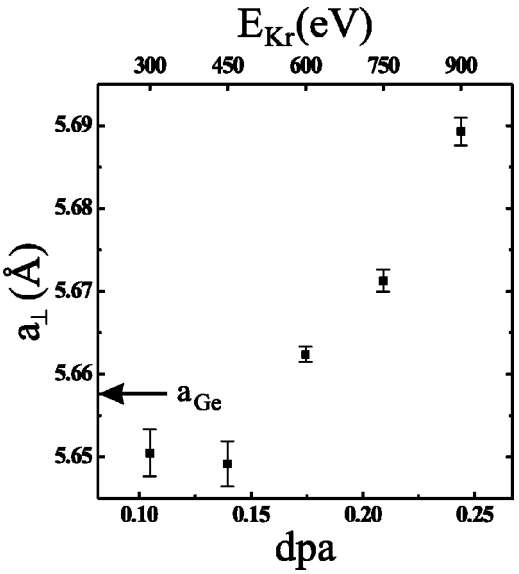

FIG. 5. Measured $Ge_{0.99}C_{0.01}$ lattice constants $a_{\perp}$ along the film growth direction for fully coherent layers deposited on Ge(001) as a function of lattice displacement per incident Ge atom (dpa). The films were grown at $T_s=300\,^{\circ}$C by Kr^{+} ion-beam sputtering with $E_{Kr}=300-900$ eV.

$=0.18$) leads to compressive strain, which continues to increase with increasing E_{Kr}. In contrast, as noted in Sec. II, pure Ge layers deposited under the same conditions exhibited no residual strain. Thus, the large changes observed in the strain state of the alloy layers as a function of dpa, together with the *ab initio* results presented above and the fact that all alloy layers are fully coherent with the substrate, clearly indicate that the C atom lattice site distribution in $Ge_{1-y}C_y(001)$ alloys is mediated by irradiation-induced defects due to hyperthermal Ge. We use the measured macroscopic strain together with our calculated lattice strain coefficients α and formation energies U to analyze C lattice site distributions in $Ge_{1-y}C_y(001)$ as a function of Ge hyperthermal irradiation.

As shown in Fig. 5, layers grown with $E_{Kr} \leqslant 450$ eV (dpa$\leqslant 0.14$) exhibit a nearly constant tensile strain with $a_\perp \simeq 5.65$ Å suggesting that hyperthermal irradiation resulting in dpa values smaller than 0.14 does not play a dominant role in determining C lattice site distributions in $Ge_{0.99}C_{0.01}$. Our calculated results show that the tensile layers must have a significant fraction of incorporated C atoms residing on substitutional sites since the other low-energy configurations lead to compression. We attribute the presence of substitutional C in these alloys, even though C pairs have a slightly-lower formation energy, to kinetic limitations on the C–C encounter probability imposed by the relatively low C concentration and growth temperature used in these experiments. The substitutional C fraction cannot be 100%, however, since fully substitutional C would yield $a_\perp = 5.617$ Å, lower than we observe. Assuming that the films contain only substitutional C atoms and C pairs, the two lowest-energy configurations, we estimate from Eq. 1, using our calculated strain coefficients and the measured alloy lattice constant, that 65% of the C atoms occupy pair sites while 35% are incorporated into substitutional sites.

$Ge_{0.99}C_{0.01}(001)$ films grown with dpa values >0.14 are under compressive strain, with $a_\perp$ increasing from 5.662 Å for layers with dpa$=0.18$ ($E_{Kr}=600$ eV) to 5.689 Å with dpa$=0.24$ ($E_{Kr}=900$ eV). The compressive strain in these layers is too large to be accounted for by C incorporated solely in substitutional and C pair sites. The maximum alloy lattice constant in this case, corresponding to 100% incorporation as C pairs, is only $a_\perp = 5.668$ Å while measured $a_\perp$ values are significantly higher. We attribute the increasingly large compressive strains in layers grown with dpa values >0.14 to an increasing fraction of C incorporated in Ge–C split interstitials as a result of the defect-mediated mechanism described below. However, complete C incorporation in Ge–C split interstitials would correspond to an alloy lattice constant of $a_\perp = 5.711$ Å, which is larger than we observe.

The Ge–C split interstitial forms as a substitutional C atom traps a Ge self-interstitial, Ge_i. A similar reaction path was reported in electron-irradiated C-implanted Si where Si self-interstitials produced by the electron bombardment reacted with substitutional C atoms to produce Si-C split interstitials.[26] As in the case of Si:C, the Ge–C split interstitial configuration, with a formation energy per C atom, 1.95 eV and 1.78 eV higher than that of C pairs and substitutional C, respectively, becomes energetically favorable in the presence of Ge self-interstitials. The Ge–C split interstitial formation energy associated with the combination of substitutional C and Ge_i is -1.2 eV. Thus, the Ge–C split interstitial formation probability during film growth depends upon growth kinetic factors controlling the concentrations and mobilities of substitutional C atoms and Ge_i.

In our experiments, both the $Ge_{0.99}C_{0.01}(001)$ compressive strain (Fig. 5) and the dpa [Fig. 2(b)] increase approximately linearly with E_{Kr}. We therefore conclude that the Ge self-interstitial concentration is directly proportional to the dpa (for dpa>0.14) as a direct result of hyperthermal Ge irradiation.

We expect the C pair concentration to be a function primarily of film growth temperature and, to first order, independent of E_{Kr}. Increasing E_{Kr} will, however, result in a slight decrease in the C pair concentration due to the corresponding increase in film growth rate. The primary effect of raising E_{Kr}, however, is to increase the fraction of hyperthermal Ge atoms incident on the growing film with sufficient energy to produce lattice displacements. This, in turn, converts an increasing fraction of substitutional C atoms into Ge–C split interstitials. In the limiting case for which all substitutional C atoms ($y_{sub} \simeq 0.0035$) trap Ge self-interstitials, we calculate an out-of-plane lattice parameter, assuming that the C pair concentration ($y_{pair} \simeq 0.0065$) remains constant, of $a_\perp = 5.682$ Å in very good agreement with our measured value, $a_\perp = 5.689$ Å, for $Ge_{0.99}C_{0.01}$ alloy layers grown with the highest dpa, 0.24.

V. CONCLUSIONS

In summary, our experimental results, coupled with *ab initio* calculations and TRIM simulations, show that fast sputtered Ge atoms during the epitaxial growth of fully strained $Ge_{0.99}C_{0.01}$ by UHV ion-beam sputter deposition on Ge(001) at $T_s = 300\,^\circ$C strongly affect the distribution of incorporated C atoms. This is manifested as a large change in the measured macroscopic strain. All $Ge_{0.99}C_{0.01}$ alloys, irrespective of sputtering conditions, are fully coherent with their Ge(001) substrates. Layers grown at low Kr^+ ion energies, such that the energy distribution of incident Ge atoms, corresponding to a dpa$\leqslant 0.14$ are under tensile strain with C atoms incorporated in both substitutional and C pair sites. At higher E_{Kr} leading to dpa values >0.14, the increasing concentration of Ge self-interstitials produced by fast sputtered Ge atom irradiation results in the conversion of an increasing fraction of substitutional C atoms to Ge–C split interstitials. This, in turn yields additional in-plane compressive strain that increases approximately linearly with increasing dpa.

ACKNOWLEDGMENTS

The authors gratefully acknowledge the financial support of the Materials Science Division of the Department of Energy under Contract No. DEFG02-96ER45439. We also appreciate the use of the facilities at the Center for Microanalysis of Materials, which is partially supported by DOE, at the University of Illinois. J.D.-G. was partially supported by the Natural Sciences and Engineering Research Council (NSERC) of Canada, and P.D. was partially supported by NSERC and the Fonds pour la Formation de chercheurs et à l'aide à la recherche (Québec, Canada).

[1] D. M. Mattox and G. J. Kominiak, J. Vac. Sci. Technol. **9**, 528 (1972).
[2] G. Håkansson, J. E. Sundgren, D. McIntyre, J. E. Greene, and W.-D. Münz, Thin Solid Films **153**, 55 (1987).
[3] F. Adibi, I. Petrov, J. E. Greene, L. Hultman, and J.-E. Sundgren, J. Appl. Phys. **73**, 8580 (1993).
[4] T. Michely and G. Comsa, Phys. Rev. B **44**, 8411 (1991).
[5] J. E. Greene, J.-E. Sundgren, L. Hultman, I. Petrov, and D. B. Bergstrom, Appl. Phys. Lett. **67**, 2928 (1995).
[6] S. Berg and I. V. Katardijev, J. Vac. Sci. Technol. A **17**, 1916 (1999).
[7] M. A. Hasan, J. Knall, S. A. Barnett, J.-E. Sundgren, L. C. Markert, A. Rockett, and J. E. Greene, J. Appl. Phys. **65**, 172 (1989).
[8] W.-X. Ni, J. Knall, M. A. Hasan, G. V. Hansson, J.-E. Sundgren, S. A. Barnett, L. C. Markert, and J. E. Greene, Phys. Rev. B **40**, 10 449 (1989).
[9] I. Petrov, L. Hultman, U. Helmersson, J.-E. Sundgren, and J. E. Greene, Thin Solid Films **169**, 299 (1989).
[10] I. Petrov, L. Hultman, J.-E. Sundgren, and J. E. Greene, J. Vac. Sci. Technol. A **10**, 265 (1992).
[11] M. Kitabtake, P. Fons, and J. E. Greene, J. Vac. Sci. Technol. A **8**, 3726 (1990).
[12] M. Kitabatake and J. E. Greene, J. Appl. Phys. **73**, 3183 (1993).
[13] N.-E. Lee, G. Xue, and J. E. Greene, J. Appl. Phys. **80**, 769 (1996).
[14] G. A. Tomasch, Y.-W. Kim, L. C. Markert, N.-E. Lee, and J. E. Greene, Thin Solid Films **223**, 212 (1993).
[15] See for example C. J. Tsai, H. A. Atwater, and T. Vreeland, Appl. Phys. Lett. **57**, 2305 (1990).
[16] A similar dependency has been reported for C in $Si_{1-x}Ge_x$ alloy layers where C atoms interact with Si self-interstitials to form split-interstitial complexes and consequently reduce B diffusion in *npn* bipolar heterojunction transistors. See H. J. Osten, B. Heinemann, D. Knoll, G. Lippert, and H. Rücker, J. Vac. Sci. Technol. B **16**, 1750 (1998).
[17] J. D'Arcy-Gall, P. Desjardins, I. Petrov, J. E. Greene, J.-E. Paultre, R. A. Masut, S. C. Gujrathi, and S. Roorda, J. Appl. Phys. **88**, 96 (2000).
[18] N.-E. Lee, M. Matsuoka, M. R. Sardela, Jr., F. Tian, and J. E. Greene, J. Appl. Phys. **80**, 812 (1996).
[19] X.-J. Zhang, G. Xue, A. Agarwal, R. Tsu, M.-A. Hasan, J. E. Greene, and A. Rockett, J. Vac. Sci. Technol. A **11**, 2553 (1993).
[20] J. P. Noel, N. Hirashita, L. C. Markert, Y.-W. Kim, J. E. Greene, J. Knall, W.-X. Ni, M. A. Hasan, and J.-E. Sundgren, J. Appl. Phys. **65**, 1189 (1989).
[21] R. M. Dreizler and E. K. U. Gross, *Density Functional Theory* (Springer-Verlag, Berlin, 1990).
[22] J. P. Perdew and Y. Wang, Phys. Rev. B **45**, 13 244 (1992).
[23] J. F. Ziegler, J. P. Biersack, and U. Littmark, *Stopping and Ranges of Ions in Solids* (Pergamon Press, New York, 1985).
[24] D. K. Brice, J. Y. Tsao, and S. T. Picraux, Nucl. Instrum. Methods Phys. Res. B **44**, 68 (1989).
[25] In order to evaluate the suitability of TRIM simulations, we performed calculations for Si irradiation with Ar^+ and compared the results with previously published molecular dynamics simulations of atomic displacements during 10–50 eV Ar irradiation of Si(001)2×1 [H. Gnaser, *Low-Energy Ion Irradiation of Solid Surfaces* (Springer-Verlag, Berlin, 1999)]. Reasonable agreement was obtained for the number of displacements below the second atomic layer. We therefore expect our TRIM calculations to be at least qualitatively valid and to predict the correct trends for interpreting the effects of fast sputtered neutrals on film growth.
[26] G. Davies and R. C. Newman, in *Handbook on Semiconductors*, edited by S. Mahajan (Elsevier, New York, 1994), Vol. 3, p. 1557.